Journal of Volcanology and Geothermal Research 274 (2014) 108–121

Contents lists available at ScienceDirect

Journal of Volcanology and Geothermal Research

journal homepage: www.elsevier.com/locate/jvolgeores

Mt. Etna 2001 eruption: New insights into the magmatic feeding system and the mechanical response of the western flank from a detailed geodetic dataset

Pablo J. González [a,*], Mimmo Palano [b]

[a] Department of Earth Sciences, University of Western Ontario, Biological and Geological Sciences Building, London, Ontario N6A 5B7, Canada
[b] Istituto Nazionale di Geofisica e Vulcanologia, Osservatorio Etneo — Sezione di Catania, Piazza Roma, 2, 95123 Catania, Italy

ARTICLE INFO

Article history:
Received 28 June 2013
Accepted 7 February 2014
Available online 14 February 2014

Keywords:
2001 Mt. Etna eruption
GPS
InSAR
Modelling
Atmospheric correction
Coulomb stress changes

ABSTRACT

In the last decades, the increasing availability of comprehensive geodetic datasets has allowed for more detailed constraints on subsurface magma storage and conduits at several active volcanoes worldwide. Here, by using a large dataset of geodetic measurements collected between early January 2001 and August 2001, we identified at least six different deformation stages that allow us to quantify the surface deformation patterns before, during and after the 2001 Mt. Etna volcanic eruption. Our results are largely in agreement with previous works (*e.g.* the presence of a deep inflating source and a shallow dike located beneath the north-western and upper southern flanks of the volcano, respectively). However, we provide (1) finer resolution of the temporal activity of these magmatic sources, leading to (2) new evidence related to the evolution of the magmatic system and the mechanical response of the western flank, in particular during the pre-eruptive phase. Results and analysis show a clear change in the ground deformation pattern of the volcano in response to the 20–24 April 2001 seismic swarm that occurred beneath the western flank, evolving from a volcano-wide inflation to a slight deflation of the summit area. We suggest that the source responsible for the volcano-wide inflation, beginning in the fall of 2000, experienced a drastic reduction in the inflation rate in response to this seismic swarm. Moreover, we provide evidence for the presence of a new inflating source located beneath the upper southern flank at a depth of ~7.0 km bsl that triggered both the occurrence of the 20–24 April 2001 seismic swarm and led to the rapid ascent of magma upward to the surface after 12 July (the Lower Vents system was fed by fresh magma rising from this source). The presence of this inflating source is inferred by (1) seismological and volcanological observations coming from the 2001 eruption and (2) seismological constraints coming from a previous similar episode that occurred at Etna during the 1993–1998 period. Furthermore, both shallow deflations observed after the 20–24 April 2001 seismic swarm and during the first day of the eruption also could be due to the deflation of two adjacent portions of the same shallow (~2 km bsl) reservoir. Such reservoirs would feed the activity that occurred at the South-East Crater after January 2001 and the activity of the Upper Vents system during the July–August eruption, in agreement with petrochemical observations. Through an updated revision of the available data, we shed some light on the relevance of pre-eruptive activity patterns, an important element for an effective volcano monitoring.

1. Introduction

The rapid growth in continuous GPS networks and improvements in Interferometric Synthetic Aperture Radar (InSAR) imaging in the last two decades allow for the acquisition of both continuous and spatially extensive datasets at an increasing number of volcanoes worldwide. These datasets are able to capture, with high resolution, the deformations accompanying pre-eruptive inflation, dike intrusion and co-eruptive deflation. When combined with appropriate source models, they can provide important constraints on subsurface magma storages and conduits (*e.g.* Lisowski et al., 2008; Fukushima et al., 2010; Montgomery-Brown et al., 2011; Palano et al., 2012; González et al., 2013).

Nowadays, Mt. Etna (Italy) and Kīlauea (Hawaii) are considered the two best-monitored active volcanoes on Earth, due to (1) the presence of dense geodetic permanent arrays (more than 30 GPS stations) and (2) the availability of large SAR data archives, that enables one to recognize and measure both long-term (*e.g.* seaward sliding of unstable flanks) and short-term deformation episodes (*e.g.* dike intrusions) with spatially and temporally dense coverage (*e.g.* Solaro et al., 2010; Baker and Amelung, 2012; Bruno et al., 2012). For example, results coming from the modelling of these datasets have highlighted that the magmatic system at the summit of Kīlauea is not represented by a

* Corresponding author.
E-mail address: pabloj.glez@gmail.com (P.J. González).

http://dx.doi.org/10.1016/j.jvolgeores.2014.02.001
0377-0273/

simple magma chamber geometry, but rather it consists of a complex series of dikes and sills (see Baker and Amelung, 2012 and references therein). Moreover, at Mt. Etna the distribution of the ground deformation sources modelled since 1993 depicts a vertically elongated volume, bordering the NW side of a high density body detected from seismic tomography studies (*e.g.* Chiarabba et al., 2000), that is considered the preferential pathway for magma uprising (see Bonforte et al., 2008 for an overview).

Taking advantage of the availability of an extensive dataset of continuous GPS data (spanning the early January–mid August 2001 period) and an InSAR image pair (covering the 6th June–11th July 2001 period), here we revisited the July–August 2001 Mt. Etna eruption as well as the volcanic activity before and after this event, with the aim of improving the knowledge of the dynamics of the magma feeding system. This eruption represents one of the best studied eruptive events at Mt. Etna volcano and several features of this event have been inferred based on geological, volcanological, seismological, geodetic and magnetic observations (see Puglisi et al., 2008 for an overview). In particular, there is a general consensus that (1) the eruption was fed by a near vertical dike, oriented roughly N–S, located a few km south of the summit craters (*e.g.* Bonaccorso et al., 2002; Behncke and Neri, 2003; Patanè et al., 2003) and (2) two different compositions of magma were erupted: the Upper Vents system (UV) emitted products which had undergone crystallization and differentiation, while the Lower Vents system (LV) was fed by a magma that evolved under high pressure and possibly experienced a quick rise to the surface (Metrich et al., 2004; Corsaro et al., 2007). The occurrence of two different magma compositions requires the presence of at least two separate magma storage systems (a shallow one feeding the activity of the UV and a deeper one related to the activity of LV). Moreover, the ratio between selected incompatible elements suggests that both magmas derive from a deep common parental magma (Corsaro et al., 2013). Episodic GPS measurements, carried out in July 2000 and in July 2001 (just before the eruption onset) respectively, inferred the presence of an inflating source located beneath the north-western flank of the volcano at a depth of about 6.0 km bsl, proposed as the source of the deep common parental magma feeding the eruption (Puglisi et al., 2008). However, some primary aspects remain unclear such as (1) the relationship between this source and the occurrence of two seismic swarms beneath the western (in late April 2001) and southern (in May–June 2001) flanks of the volcano; (2) the ground deformation pattern in the pre-eruptive phase and (3) the lack of geodetic evidence for the shallow magmatic source feeding the UV. Better constraints on those aspects will benefit the interpretation of the entire eruption and, in particular, shed some light on the less well understood pre-eruptive phase and its role in the subsequent eruption.

To this aim, we revisited the dynamics preceding and encompassing the July–August 2001 Mt. Etna eruption by using an extensive geodetic dataset. Although continuous GPS data for certain time intervals are limited in number, we recognized at least six different ground deformation stages, providing new constraints on the evolution of the magmatic system of Mt. Etna and the mechanical response of the western flank over the entire investigated period. While some of our findings are in agreement with previous works (*e.g.* the presence of a deep pressuring source and a shallow dike located beneath the north-western and upper southern flanks of the volcano, respectively), we provide evidence for the presence of a new deep pressuring source located beneath the upper southern flank that triggered the occurrence of the late April 2001 seismic swarm and fed the LV. We infer also the presence of two deflating sources located at a shallow depth close to the summit area that fed the UV. Finally, we discussed our finding with respect to geological, volcanological and seismological observations that illuminate relevant eruptive activity patterns, in order to improve the volcano monitoring and risk management.

2. Background setting

Mt. Etna is a large Quaternary basaltic stratovolcano located on the east coast of Sicily (Fig. 1a). Since the end of the large 1991–1993 eruption, Mt. Etna has undergone a period of low volcanic activity characterized by a continuous inflation with an almost constant rate (Palano et al., 2008). Magmatic activity resumed in July 1995, at the Bocca Nuova crater (Fig. 1c), then spread alternately to the other summit craters in the following years (*e.g.* Allard et al., 2006). Starting from 1997, a sharp increase in seismicity affected the entire volcanic edifice with the occurrence of some strong swarms on 9–14th January, 1998 (western flank), on 5–8th November, 2000 (lower southern flank), on 20–24th April, 2001 (western flank), and on May–June 2001 (upper southern flank) (*e.g.* Bonaccorso et al., 2004; Bonanno et al., 2011). The increase in seismicity after January 2001 was followed by an increase of explosive activity at the summit craters, mainly concentrated at the South-East crater (SEC, Fig. 1c; Lautze et al., 2004). In particular, lava emission from a fissure that opened on the N flank of the SEC began on 21st January and proceeded at low effusion rate through late April. Throughout early May 2001 the lava effusion rate increased, often accompanied by weak spattering at the eruptive vent (Allard et al., 2006). Then, starting on 5th June, a series of 15 lava fountaining paroxysms were followed by the July–August 2001 flank eruption (Fig. 1b; Puglisi et al., 2008). This eruption was preceded by an intense seismic swarm (more than 2600 events in less than 4 days; $M_{MAX} = 3.9$) starting on the night of 12th July (Saraò et al., 2010). The earthquake hypocenters were fairly shallow (0–3 km bsl) and marked the upward propagation of a magmatic intrusion beneath the southern flank of the volcano (Bonaccorso et al., 2002). Between 13th and 19th July, a *ca.* 7 km long fracture–fissure field, striking roughly N–S and mostly parallel to the western margin of the Valle del Bove opened on the middle-upper southern flank (Fig. 1c). The higher portion of the fracture field, from 2950 m down to 2700 m asl, formed after 13th July. Vents (UV) opened along this sector after 17th July and fed lava flows spreading into the Valle del Bove and over Piano del Lago (Fig. 1b; Lanzafame et al., 2003; Acocella and Neri, 2003; Lautze et al., 2004). On 18th July, along the lower portion of the fracture field, a vent (LV) producing Strombolian activity and lava flows that expanded toward south opened at 2100 m asl. In late afternoon of 19th July, two coalescent pit craters opened at 2550 m asl (belonging to LV), on the upper southern flank, giving rise to hydromagmatic explosions. On 25th July, the activity at 2550 m became magmatic, and the fallout around the pits formed a cinder cone. After the end of July the lava flows from the UV gradually stopped. The eruption ended on 9th August 2001. Petrochemical studies proved that, although deriving from a deep common parental magma, the erupted magma from LV was more primitive than that emitted from UV, suggesting that the two fissure systems were fed by different magmas (Metrich et al., 2004; Corsaro et al., 2007, 2013). Subsequently, some authors suggested that the rise of magma from depth was primarily controlled by the N–S regional tectonic stress field, while the emplacement of the dike at a shallow depth was controlled or by the local gravitational stress field acting at the surface (*e.g.* Acocella and Neri, 2003) or by the presence of weak crust beneath the upper southern flank of the volcano (*e.g.* Carbone et al., 2009).

3. Geodetic data

On Mt. Etna, the GPS permanent network began to operate in November 2000, reaching a configuration of 13 stations in the late summer of 2001 (Fig. 1). To study the ground deformation pattern affecting Mt. Etna before, during and after the eruption, we analysed all available continuous GPS measurements collected between early January 2001 and August 2001 plus an InSAR image covering the 6th June–11th July 2001 time interval. In addition, for the July 2000–July 2001 time interval

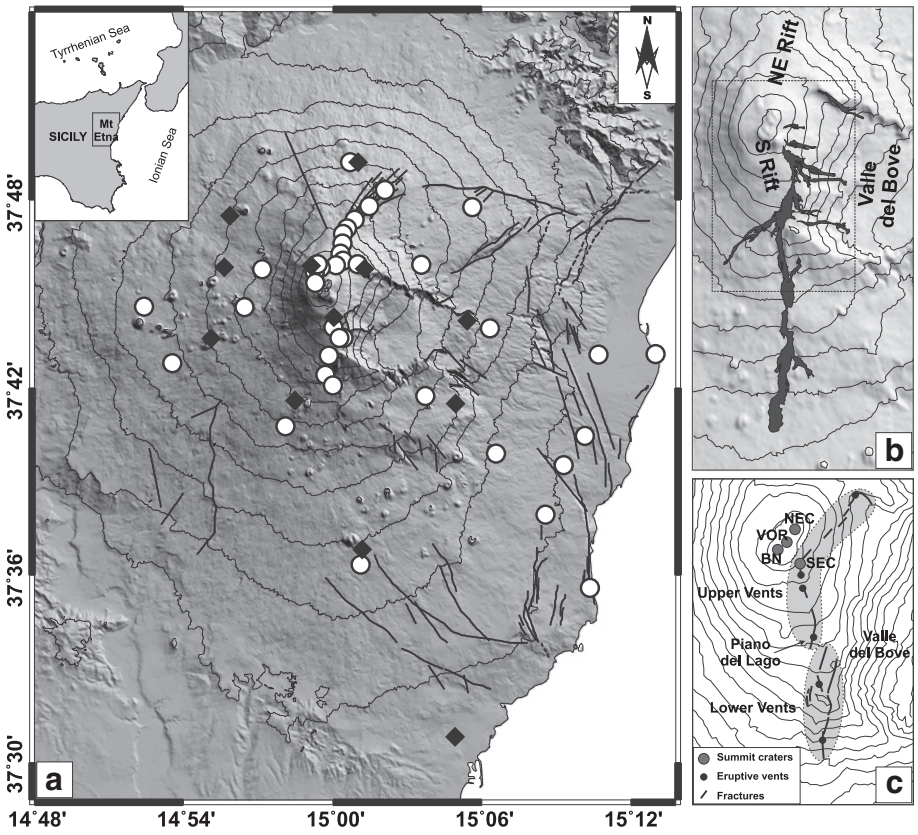

Fig. 1. a) Simplified structural map of Mt. Etna. GPS benchmarks whose displacements are analysed in this work are reported as black diamonds (continuous GPS sites) and white points (GPS benchmarks surveyed in campaign-mode). b) Map of the lava flows produced during the 2001 eruption. c) Map of the summit area of the volcano and the fissure system fields opened during the eruption onset (modified from Puglisi et al., 2008). Abbreviations are as follows: BN, Bocca Nuova; NEC, North-East Crater; SEC, South-East Crater; VOR, Voragine.

we refer to the episodic GPS measurements analysed in Puglisi et al. (2008).

3.1. InSAR data processing

At Mt. Etna, InSAR data have been used to analyse the long-term behaviour of the magmatic system (Solaro et al., 2010), and stability of the volcano (Froger et al., 2001; Lundgren et al., 2004), and to constrain models for intrusions and earthquakes that occurred during the last two decades (Palano et al., 2008; Guglielmino et al., 2011). In particular, Puglisi et al. (2008) and Lundgren and Rosen (2003) presented a comprehensive analysis of a set of differential interferograms spanning the 2001 pre-, co- and post-eruption phases. Here, we do not intend to replicate their analysis in full, but to focus our attention on the pre-eruptive phase leading to the July–August 2001 eruption.

We used the European Remote Sensing ERS-2 satellite images to place limits on the pre-eruptive volume change. Due to the failure of the gyroscopes on-board the ERS-2 satellite in fall 2000, the number of available SAR images useful for interferometry was reduced to a single coherent pre-eruptive pair in ascending orbital pass. The interferogram was processed in two-pass differential interferometry mode, using a 90-m-resolution digital elevation model derived from the Shuttle Radar Topography Mission. ERS-2 data were focused by using ROI_PAC (Rosen et al., 2004) and interferometrically processed using the Doris software package (Kampes et al., 2003). We obtained a short baseline (~313 m) differential interferogram between 6th June 2001 and 11th July 2001 (see Fig. A1a in Appendix A), just a day before the onset of the intense seismic swarm. After removal of the orbital residual trends, the 6th June 2001–11th July 2001 interferogram (Fig. A1a) shows up to 4 cm of phase change toward the satellite of the summit-to-southwest flank of the volcano. The signal is consistent with a computed interferogram shown in Fig. 4a in Puglisi et al. (2008). InSAR differential phase changes can be significantly affected by variations in water vapour concentrations at Mt. Etna (*e.g.* Delacourt et al., 1998; Beauducel et al., 2000). However, an empirical phase-elevation ratio could not be estimated without likely removing a part of the ground deformation signal. To analyse possible atmospheric phase contributions for the selected differential interferogram, we explored two independent correction models (see Appendix A for additional details), the former (Fig. A1c,e) based on MODIS (Li et al., 2005; Eff-Darwich et al., 2012), the latter (Fig. A1d,f) based on the ERA-Interim global weather reanalysis models (Jolivet et al., 2011). The MODIS-corrected differential phase shows a reverse signal (Fig. A1e), *i.e.* a general subsidence with a magnitude of ~5 cm along the LOS direction which is larger than the subsidence detected by GPS data described in the following paragraph. We think that this likely reflects variable conditions of the atmosphere between the MODIS acquisition time (~10:30) and ERS-2 SAR image acquisition time (~21:00, local time). The ERA-Interim corrected differential phase, reported on Fig. 2 (and Fig. A1f also), depicts smaller residuals. It indicates that the atmospheric contributions likely produced an apparent inflationary signal of ~4 cm. Therefore, it seems that there was little precursory deformation during the month before the eruption, as the small changes in the EGDF–EMGL GPS baseline component and the obtained atmospheric corrected interferogram indicate (Figs. 2 and 3).

3.2. GPS data processing

GPS data were processed using the GAMIT/GLOBK software (Herring et al., 2010) with IGS (International GNNS Service; http://igscb.jpl.nasa.gov) precise ephemerides. To improve the overall configuration of the network and tie the regional measurements to an external global reference frame, data coming from 10 continuously operating IGS stations (BRUS, CAGL, GENO, GRAS, GRAZ, JOZE,

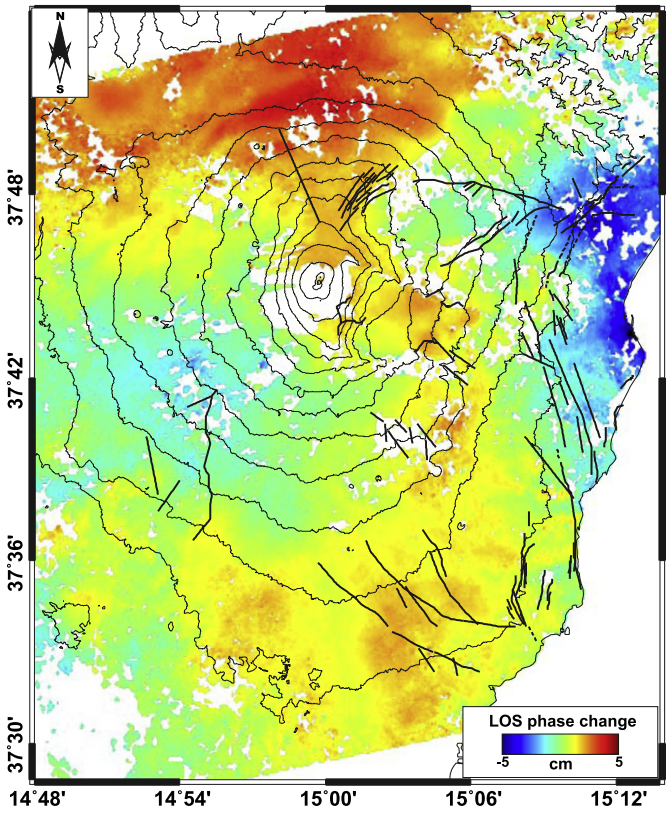

Fig. 2. ERA-Interim corrected differential phase map spanning the 6th June–11th July 2001 time interval. Areas which lack interferometric coherence are uncoloured. We use the convention that negative motion is toward the satellite.

MATE, MEDI, NOT1 and ZIMM; see Beutler et al., 2008 for details about the whole IGS stations) were introduced in the processing. In a first step, we used daily double differenced GPS phase observations to estimate station coordinates and Earth orientation parameters. In this step, the observations were weighted according to the elevation angle, for which a cut-off angle of 10° was chosen. In addition, we used the latest absolute receiver antenna models by the IGS and we adopted the Saastamoinen (1972) atmospheric zenith delay models, coupled with the Global Mapping Functions (Boehm et al., 2006) for the neutral atmosphere.

Estimated GPS daily time series and velocities/displacements for specified time intervals were referred to the "Etn@ref" reference frame (a local reference frame computed to isolate the Mt. Etna volcanic deformation from the background tectonic pattern; Palano et al., 2010) by minimizing, for the abovementioned 10 IGS stations, the difference between their estimated positions and those implied by their coordinates (position and velocity) in the local reference frame.

3.3. Ground deformation pattern at Mt. Etna

To detect significant signals related to Mt. Etna activity we analysed daily baseline changes for sites EGDF and EMGL because they were quasi-continuously operating throughout the investigated time period (Fig. 3). The visual inspection of the EGDF–EMGL baseline component allows us to detect at least five different ground deformation stages, spanning the 12th January to 15th August 2001 time interval; for each detected stage we computed the ground deformation field (Fig. 3). We also considered an additional time interval (hereinafter *I1*) which takes into account the ground deformation field computed from the comparison of episodic GPS measurements carried out in July 2000 and in July 2001 (just before the beginning of the eruption onset) respectively and previously analysed in Puglisi et al. (2008). This ground deformation field, reported on Fig. 4a,b, is characterized by a general radial pattern of surface displacements on the volcano, with an uplift of ~60 mm centred on its upper north-western flank, coupled with a slight lowering of ~15 mm of the summit area. We should note that the survey results sample the cumulative deformation occurred along a 1-year period. Analysis of the EGDF–EMGL baseline shows significant changes during this period, encompassing at least 2 different deformation phases.

In particular, from 12th January to 20th April 2001, horizontal velocities of GPS stations pointed away from an area centred a few km NW of the summit area of the volcano, clearly depicting a general inflation of the volcano edifice accompanied also by positive vertical velocities (Fig. 4c,d). The occurrence of a seismic swarm on 20th–24th April 2001 beneath the western flank of the volcano generated an offset of about 4–6 mm on the EGDF–EMGL baseline component. Because the offset is small (it is visible only on the daily time series displacement of the EMGL site due to its proximity to the seismogenic volume) and its sign is coherent with the general lengthening observed since 12th

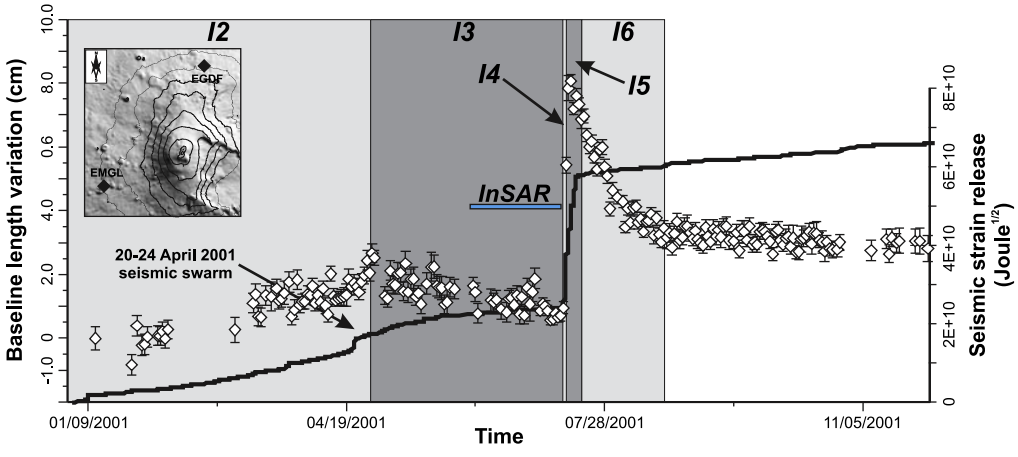

Fig. 3. Temporal evolution of the EGDF–EMGL baseline length (white diamonds) and the cumulative seismic strain release (continuous black line). The blue line shows the time interval covered by the InSAR data (Fig. 2). Interval *I1*, here not reported, refers to the ground deformation field computed from episodic GPS measurements carried out in July 2000 and in July 2001 respectively (Puglisi et al., 2008). Other intervals are as follows: *I2*, from 12th January to 24th April; *I3*, from 24th April to 12th July; *I4*, from 12th July to 13th July; *I5*, from 13th July to 18th July; and *I6*, from 18th July to 15th August. It must be noted that *I1* include *I2* and *I3* stages. Between 13th and 14th July, EGDF sites moved toward North leading to an increase of the EGDF–EMGL baseline length. However, because this motion is well-detected only at site EGDF, we prefer to consider the deformation as homogeneous across the longer 13th–18th July time interval.

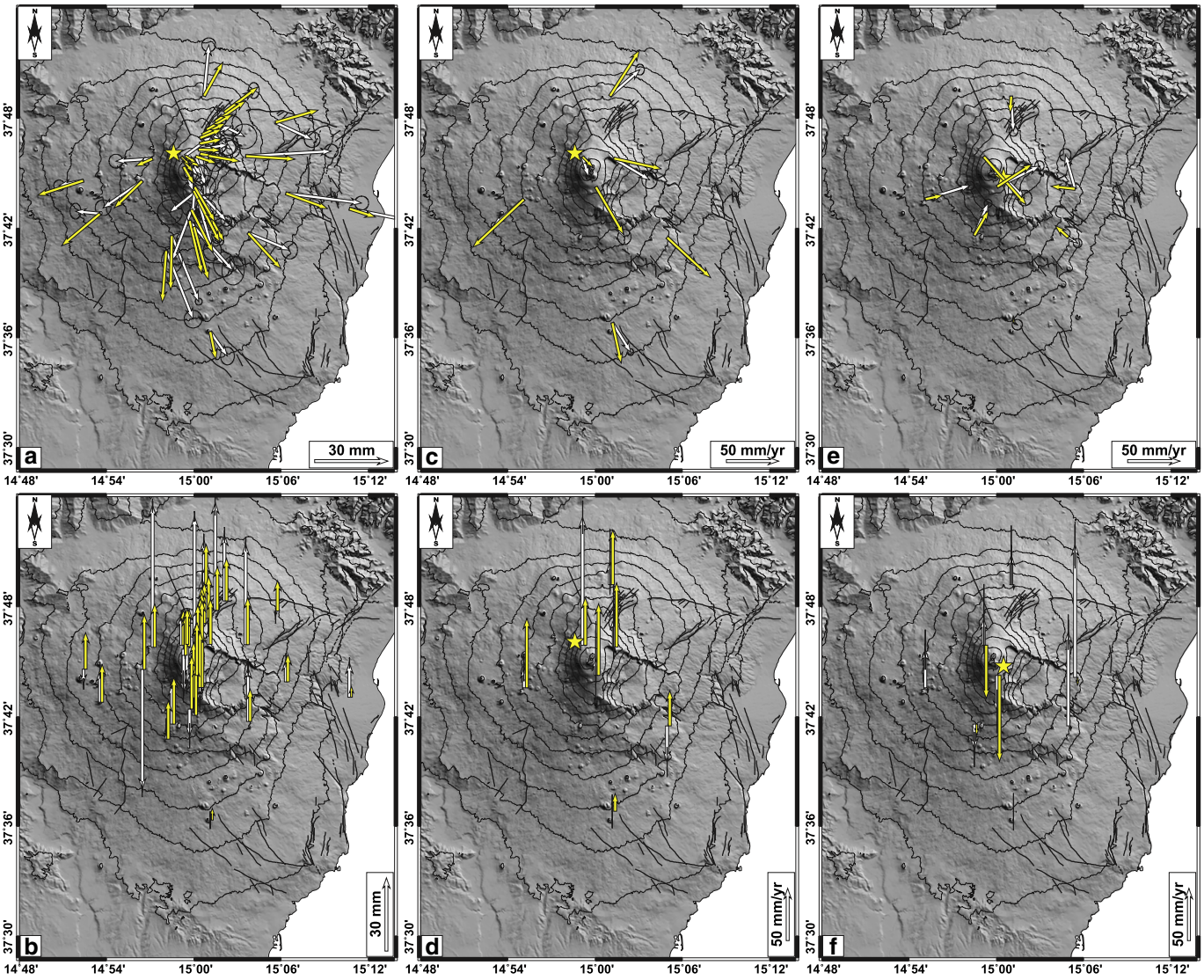

Fig. 4. Comparison between observed (white arrows) and expected (yellow arrows) horizontal (panels a, c and e) and vertical (panels b, d and f) displacements/velocities relevant to each time interval: (a,b) interval *I1*; (c,d) interval *I2*; and (e,f) interval *I3*. The geodetic velocities observed at stations located on the eastern flank of Mt. Etna during *I3* are due to the limited number of available GPS observations and cannot be considered realistic. Although these stations were excluded from the inversion, the expected velocity components were also reported. Locations of modelled sources are reported as yellow stars.

January 2001, in the following we referred to an unique time interval which spans from 12th January to 24th April 2001 (hereinafter *I2*).

After the April 2001 seismic swarm, GPS data detected the occurrence of a slight contraction of the summit area (clearly detected in the horizontal components), coupled with a complex vertical pattern, where the northern half of the volcano showed uplift while the southern half subsidence (Fig. 4e,f), according to data covering interval *I1* (Fig. 4a,b). Unfortunately, the limited number of continuous data at stations located on the eastern flank of Mt. Etna during this interval does not allow us to adequately sample the deformation on this sector of the volcano. The modest, low-rate deformation pattern seems consistent with the lack of deformation on the atmospheric corrected interferogram spanning the 6th June–11th July 2001 time interval (Fig. 2f). In the following we referred to this interval, spanning the 24th April–12th July period, as *I3*.

On the night of 12th July, an intense seismic swarm marked the emplacement of an intrusion beneath the upper southern flank of the volcano. GPS measurements showed remarkable variations between 12th and 13th July (hereinafter *I4*), especially on the horizontal components (the vertical component shows very small positive changes; from a few mm up to 25 mm). This deformation pattern depicts a clear response of the volcano edifice to the fast migration of a magma intrusion along a *ca.* N–S direction into the southern flank (Fig. 5a,b). Displacement at ETDF station was influenced by the ground fracture system opened during the eruption onset.

After 13th July, the EGDF–EMGL baseline component began to experience contraction up to 15th August 2001. On 18th July, a new vent (LV) producing Strombolian activity and lava flows that expanded toward the south, opened at 2100 m asl, followed the next day by the opening of a vent further upslope, at 2550 m (belonging to LV; Lanzafame et al., 2003). Taking into account this event, we divided this time interval into two sub-intervals: interval *I5* spans from 13th to 18th July, while interval *I6* spans from 18th July to 15th August. During interval *I5*, the overall deformation field depicts a complex pattern resulting from the effects of the shallow intrusion (Fig. 5c) coupled with a deflation of the volcano edifice (as evidenced by the negative height variations at some stations located close to the summit area; Fig. 5d). During interval *I6*, the

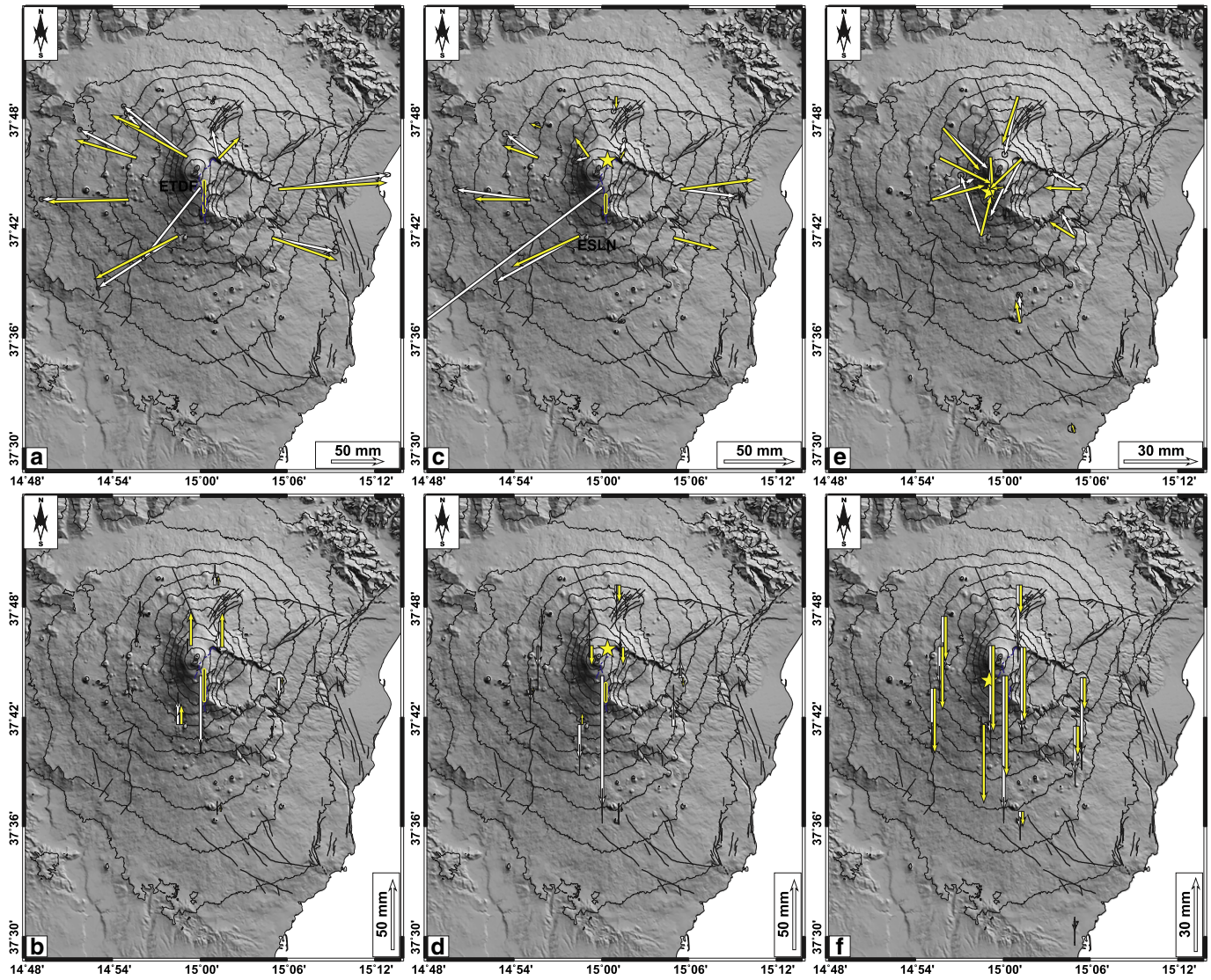

Fig. 5. Comparison between observed (white arrows) and expected (yellow arrows) horizontal (panels a, c and e) and vertical (panels b, d and f) displacements/velocities relevant to each time interval: (a,b) interval *I4*; (c,d) interval *I5*; and (e,f) interval *I6*. Locations of modelled sources are reported as yellow stars (inflating sources) and lines (dikes).

ground deformation pattern shows a clear volcano-wide deflation (Fig. 5e,f). After 15th August 2001, the EGDF–EMGL baseline length showed no significant changes for the remaining part of 2001 (Fig. 3).

4. Ground deformation modelling

The surface ground deformation field for each time interval was used as input to constrain isotropic half-space elastic inversion models. Since high temperature gradients are typically present in volcanic areas (hundreds of degrees per kilometre) and the medium is likely to behave inelastically over long time scales, the elastic approximation could be inappropriate. However, the choice to consider an isotropic and elastic medium, common to most works on volcanic deformation modelling, is usually justified because small displacement gradients are observed (*e.g.* Cayol and Cornet, 1998). Furthermore, the fairly good fit between observed and modelled ground deformation indicates that the behaviour of the volcano at the timescales analysed in this study can be considered compatible with elastic behaviour. Values of 30 GPa and 0.25 were assumed for the shear modulus and Poisson's ratio in the half-space, respectively. The rigidity chosen corresponds to a typical value of crustal rigidity commonly used in modelling works (*e.g.* Williams and Wadge, 2000; Trasatti et al., 2003; Walter et al., 2005), which has been found to be an average rigidity value for Mt. Etna crust (Chiarabba et al., 2000). The inversions were performed by using the genetic algorithm approach. To account for the effects of topography we included into the computation the method of Williams and Wadge (2000). To model the observed ground deformation pattern, we adopted the Mogi (1958) and/or the Okada (1985) and/or the Yang et al. (1988) analytical models. Estimation of the uncertainties in best-fitting parameters was performed by adopting a Jackknife sampling method (Efron, 1982). In the computation, both horizontal and vertical GPS components were inverted by taking into account weights proportional to the associated displacement errors.

4.1. Modelling of ground deformation measured before the 2001 eruption

The ground deformation pattern preceding the eruption onset (*I1*) was previously analysed in Puglisi et al. (2008). In particular, those authors inferred the presence of a spherical pressuring source, located beneath the western flank of the volcano at a depth of *ca.* 6 km bsl. Using the GPS dataset reported in Puglisi et al. (2008) we

Table 1
Parameters of the modelled sources inferred for intervals *I1* and *I3*. Strike and plunge angles are measured anticlockwise from north and clockwise from horizontal respectively. a and b are the lengths of the major and the minor axes of the prolate spheroidal source (Yang et al., 1988), respectively. ΔV is expressed as total volume changes and is calculated according to Tiampo et al. (2000). Errors (at 95% of confidence) also are reported for each parameter.

Parameters	*I1*	*I3*
Easting (km)	497.965 ± 0.351	500.936 ± 0.497
Northing (km)	4180.201 ± 0.235	4177.270 ± 0.214
Depth (km)	7.44 ± 0.69 bsl	1.86 ± 0.48 bsl
a axis (m)	1156 ± 145	
b/a ratio	0.15 ± 0.03	
Strike (°)	11 ± 12	
Plunge (°)	97 ± 4	
ΔP (Pa)	$4.32 \pm 0.11 \cdot 10^9$	
ΔV (m^3)	$15.7 \cdot 10^6$	$1.16 \pm 0.21 \cdot 10^6$

performed a new inversion, assuming a prolate spheroidal pressure source (Yang et al., 1988). The best result (RMS = 14.8 mm) is given by a near vertical elongated ellipsoidal source centred at a *ca.* 7.4 km depth beneath the upper western flank of the volcano (see Fig. 4a,b and Table 1 for details), slightly improving the fit to the observed data with respect to results obtained by Puglisi et al. (2008) (RMS = 19.3 mm).

The ground deformation field detected for time interval *I2* shows a pattern very similar to the one measured for *I1*. Because the deformation field for *I2* is sampled by very few observations and no stations cover the north-western flank of the volcano adequately, we prefer to compared it with the expected field for the best model resulting from the inversion for *I1* (Fig. 4c,d). The comparison between the observed and expected deformation field is good (RMS = 9.7 mm). providing evidence that the source active during interval *I1* adequately represents the bulk of the ground deformation measured during *I2*.

As mentioned previously, interval *I3* is characterized by the occurrence of a slight contraction of the summit area. Observed GPS velocities were inverted by adopting the Mogi (1958) model. The best result (RMS = 12.2 mm) is given by a deflating source located at ~1.8 km bsl beneath the summit area of the volcano (see Fig. 4e,f and Table 1 for details). Again, as discussed previously, because the deformation observed at stations located on the eastern flank of Mt. Etna is not considered realistic, we excluded them from the inversion. The fit between observed and modelled ground deformation is good for the horizontal components. However, it is not good for the vertical component, probably due to the complex deformation pattern detected for this time interval.

4.2. Modelling of ground deformation measured during the 2001 eruption onset

The ground deformation detected for *I4* depicts the occurrence of an intrusion beneath the upper southern flank of the volcano. The inversion was performed by assuming the Okada (1985) model. In this computation, we excluded the displacement measured at ETDF station since it is located close to the surface fracture field and its motion cannot be considered purely elastic. The best solution (RMS = 9.2 mm) is given by a tensile dislocation (estimated opening is ~2.7 m) N–S-oriented, located just below (at ~0.5 km asl) the fracture field that opened at the surface of the southern flank of the volcano (see Fig. 5a,b and Table 2 for details).

As previously mentioned, *I5* shows a complex pattern as a result of the cumulative effect of the shallow intrusion (well-depicted by horizontal displacements) and a deflation of the volcano (visible as a spatially coherent vertical displacement pattern at several GPS sites). Starting from the model obtained for *I4*, we added a pressure source into the computation, since preliminary inversions taking into account the tensile dislocation alone failed to explain the vertical displacement pattern observed at stations located on the NW sector of the volcano. Recently, the superposition of analytical models was analysed and proven valid for the model applied on this phase, a point source located along a tensile dislocation strike direction (Pascal et al., 2013). In order to avoid inverting too many parameters, the position, dimensions, dip and azimuth of the tensile dislocation were fixed to the results of the previous inversions. We inverted only its opening component, while all the parameters for the pressure source were left completely free during the inversion. In this computation we also excluded the displacements measured at ETDF station. The best solution (RMS = 12.4 mm) is given by the tensile dislocation and shows a reduction of the opening component, which decreased from ~2.7 to ~1.5 m from a deflating source located close to the summit area and at a depth of ~1.8 km bsl (see Fig. 5c,d and Table 2 for details).

4.3. Modelling of ground deformation measured after the 2001 eruption onset

The *I6* phase is clearly dominated by a volcano-wide deflation. To model the deformation pattern we adopted again the Mogi (1958) model. The best solution (RMS = 8.4 mm) depicts a deflating source located beneath the upper southern flank of the volcano at a depth of ~7.2 km bsl and characterized by a volume reduction of $\sim 13 \cdot 10^6$ m^3 (see Fig. 5e,f and Table 2 for details).

4.4. Modelling of the intrusion process using a distributed opening approach

In order to investigate the evolution of the magma propagation process during the intrusion of the eruptive feeding dike, we resolved for the variable opening distribution on the modelled dike for phases *I4* and *I5*. We subdivided the dike into patches 200 m in length by 200 m in depth and applied a damped least squares algorithm to solve for opening. We extended the obtained dike geometry in the length and depth directions to 6 km × 6 km (Fig. 6). Surface deformation (d) then can be related linearly with the dike opening distribution (s) on the fault as, $d = G\,s + error$, through forward modelling of Green's functions (G) (Okada, 1985). An optimal solution is obtained by jointly

Table 2
Parameters of modelled sources inferred for intervals *I4*, *I5* and *I6*. ΔV is expressed as total volume changes. For each parameter, errors (at 95% of confidence) also were reported.

Parameters	*I4*	*I5*		*I6*
Easting (km)	500.493 ± 0.156	500.493 (fixed)	500.619 ± 0.521	498.621 ± 0.361
Northing (km)	4175.770 ± 0.203	4175.770 (fixed)	4179.580 ± 0.509	4176.346 ± 0.335
Depth (km)	0.46 ± 0.61 asl	0.46 (fixed)	1.8 ± 0.38 bsl	7.2 ± 0.42 bsl
Strike (°)	0.1 ± 2.5	0.1 (fixed)		
Dip (°)	89.9 (fixed)	89.9 (fixed)		
Length (m)	3058 ± 168	3058 (fixed)		
Width (m)	1557 ± 297	1557 (fixed)		
Opening (m)	2.77 ± 0.51	1.51 ± 0.12		
ΔV (m^3)			$-1.8 \pm 0.64 \cdot 10^6$	$-13.0 \pm 1.17 \cdot 10^6$

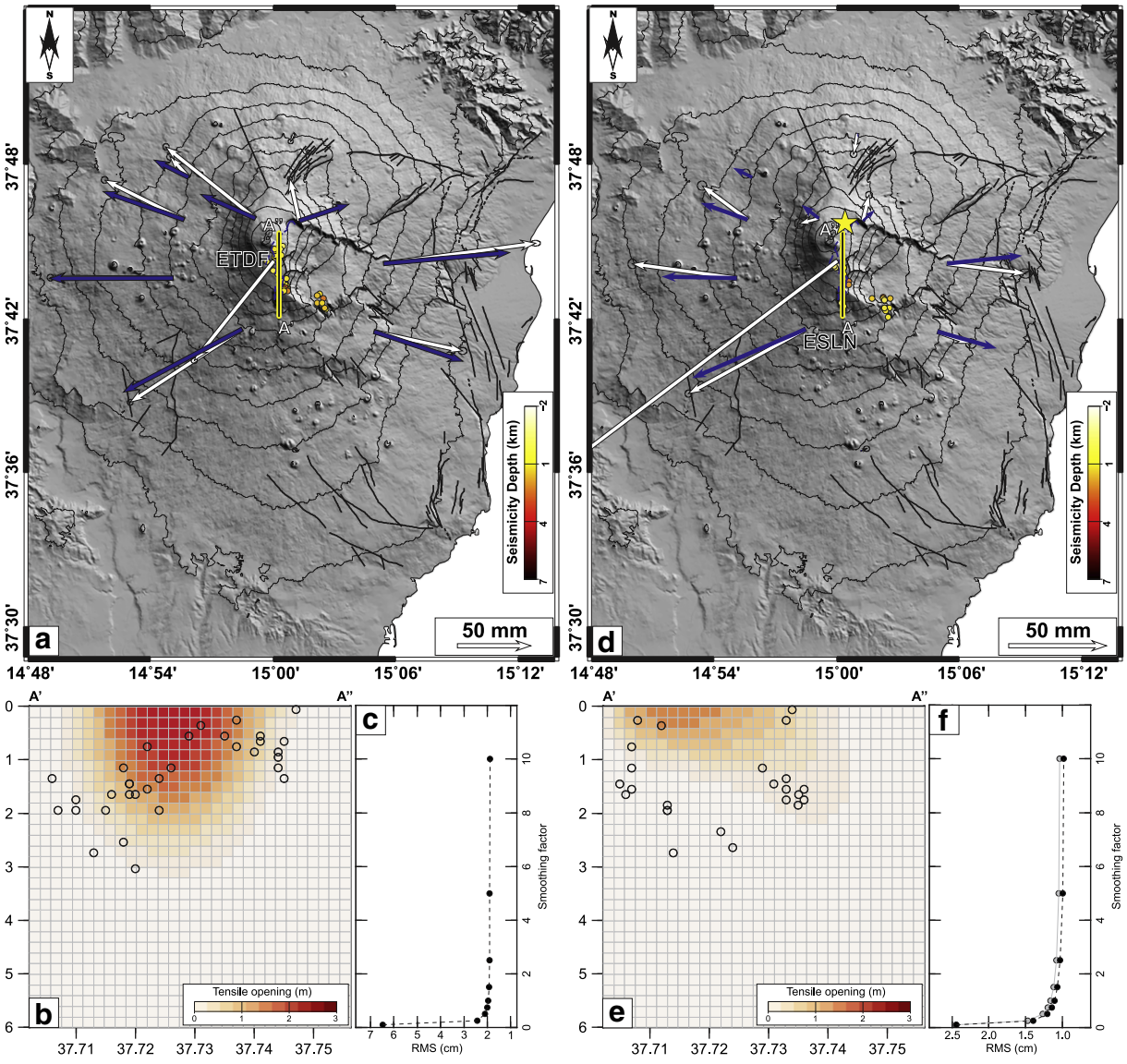

Fig. 6. Results coming from the distributed opening modelling approach: observed (white arrows) and expected (blue arrows) horizontal displacements relevant to intervals *I4* (a) and *I5* (d). Modelled sources are reported as yellow stars (inflating sources) and lines (dikes). Tensile opening component distribution along the vertical dike for intervals *I4* (b) and *I5* (e). Trade-off curve (L-curve method; Aster et al., 2005) used for the estimation of the smoothing parameter (resulting in $\kappa = 1$) for intervals *I4* (c) and *I5* (f). For both intervals, a selected dataset of earthquakes relocated using a 3D velocity model also were plotted (Saraò et al., 2010). As previously mentioned, more than 2600 events occurred from 12th July until 18th July 2001. However, due to the presence of high tremor amplitude and of coda waves from previous events which masked the first P-wave arrivals, only a part of the recorded seismicity was well-located (Saraò et al., 2010).

minimizing the data misfit and applying a damping factor (κ) to the finite difference approximation of the Laplacian as a smoothing operator, which reduces unreliable strong spatial heterogeneities in the dike opening (s). The optimal damping factor is determined using a trade-off curve to obtain a compromise value between data misfit and amount of smoothing in the dike opening distribution. We choose the L-curve method for the estimation of the smoothing parameter, resulting in $\kappa = 1$ (Aster et al., 2005).

Results obtained for phases *I4* and *I5* are reported in Fig. 6 as horizontal displacement maps (Fig. 6a,d), opening distributions along the modelled dike (Fig. 6b,e) and L-curve plots used for the smoothing parameter estimation (Fig. 6c,f). For phase *I4*, the tensile opening is restricted to the upper central portion of the dike, reaching the value of 2.65 m in the shallower patches. In addition, the overall dimension (~3 km in length and ~2.5 in width) depicted by all patches having non-zero opening agrees well with the dimension of the dike modelled by using the uniform slip approach (see Subsection 4.2 for further details). For phase *I5*, all patches having non-zero opening depict an area which is ~3 km long and ~1 km wide and located on the upper southern half of the dike, reaching the value of 1.74 m close to the surface. This aspect is in good agreement with the field observations (*e.g.* Lanzafame et al., 2003), which mapped the southward propagation of the fracture field that opened on the first day of the eruption onset. The belt depicted by the patches having non-zero opening partially overlaps with the dike modelled by using the uniform slip approach (see Subsection 4.2 for further details) and provides a slightly improved fit to the displacements observed at the stations located close to the southern tip of the dike (see the Supplementary Material section for details).

5. Discussion

In the following we discuss our main findings with respect to previous geodetic studies and geological, volcanological and seismological observations.

5.1. The pre-2001 eruption onset

The inversion for the ground deformation field spanning the 1-year time interval (*i.e.* from July 2000 to July 2001) before the Mt. Etna eruption onset infers the presence of a vertically oriented cigar-shaped inflating source located at a depth of ~7.4 km beneath the upper western flank of the volcano (Fig. 4a,b). While the horizontal position of our source is very close to the one inferred by Puglisi et al. (2008), it is ~1.2 km deeper. These difference could be due to the different analytical source models adopted (those authors adopted McTigue's (1987) model) and/or to the fact that we included an approximation of the topographic effect (Williams and Wadge, 2000). This source is located in the same vertically elongated volume depicted by the distribution of the ground deformation sources modelled over time since 1993, bordering the NW side of an high density body detected from recent seismic tomography studies (*e.g.* Chiarabba et al., 2000; Aloisi et al., 2002), and which is suggested as the preferential pathway for magma uprising (see Bonforte et al., 2008 for an overview).

However, as evidenced by a significant length variation on the EGDF–EMGL baseline, this time interval encompasses at least 2 different deformation phases of the volcano. In the first phase, spanning the 12th January–24th April 2001 period, the ground deformation field shows a pattern similar to the one observed for the July 2000–July 2001. The source inferred for this last period adequately represents the bulk of the ground deformation measured during 12th January–24th April 2001. It is likely that the magmatic recharge started in the fall of 2000, as evidenced by seismological and volcanological observations (see Puglisi et al., 2008 for an overview), but the lack of available continuous observations does not permit constraining this temporal relationship.

The 20th–24th April 2001 seismic swarm occurring below the western flank of the volcano depicted a *ca*. N50°E-oriented narrow volume characterized by a right strike-slip motion (Bonaccorso et al., 2004). The occurrence of this seismic swarm marked a clear change on the magmatic system of Mt. Etna. In particular, InSAR and GPS measurements covering approximately the 24th April–12th July period detected only a slight contraction of the summit area related to the deflation of a source located at ~1.8 km bsl beneath the south-eastern sector of the summit area (Fig. 1c). Because any clear geodetic signal related to the activity of the deep inflating source inferred for the previous period can be easily recognized, we suggest that this source experienced a sharp reduction of the inflation rate in response to the 20th–24th April 2001 seismic swarm striking the western flank of the volcano. The deflation detected close to the summit area reflects magma drainage due to the increase of volcanic activity that occurred at SEC in June–July 2001 (Lautze et al., 2004). In addition, petrologic studies carried out on products erupted during the January–July 2001 period estimated a magma stagnation zone located at a shallow depth (~2 km bsl; Corsaro et al., 2013), in good agreement with the depth inferred by our model. A slight compositional shift toward a more primitive magma was observed on products erupted during June–July 2001 by SEC, suggesting a possible mixing with a primitive magma rising from a deep source (presumably the one inferred for *I1–I2*; Corsaro et al., 2013).

5.2. The co- and post-2001 intrusion onset

The emplacement of a shallow magmatic intrusion beneath the upper southern flank of the volcano is well characterized by the displacement field measured between 12th and 13th July 2001. Results coming from the formal inversion of the observed deformation pattern infer a N–S-oriented dike, located just below the fracture field opened along the southern upper flank of the volcano at a depth of ~0.5 km asl. Parameters of the dike modelled in this study (*i.e.* position, length, width, strike, dip and opening) have similar values to those reported in Puglisi et al. (2008) obtained through the inversion of episodic measurements spanning the July–September 2001 time interval. Moreover, our results for the modelled dike differ that it is located ~0.6 km westward with respect to the one modelled by Bonaccorso et al. (2002), just below the fracture field opened at the surface of the southern flank of the volcano. This result infers a vertical propagation of the intrusion toward the surface, without requiring a deflection to explain the different locations between the modelled dike and the fracture field as proposed by Bonaccorso et al. (2010). In addition, the dike location is the same as the volume depicted by the seismic swarm that occurred between 12th and 13th July (Saraò et al., 2010). Furthermore, the dike location also falls on an anomalous volume located beneath the upper southern flank (in a depth range between the surface and 1 km bsl) and characterized by low seismic attenuation of P wave values (Martinez-Arevalo et al., 2005).

Interpretation of the results obtained by both uniform and distributed slip approaches suggests that the intrusion started at a shallow depth (~2.5 km bsl) and propagated vertically toward the surface, reaching a maximum tensile opening of ~2.7 m (~0.8 m less than the opening estimated by Bonaccorso et al., 2002) centred beneath the Piano del Lago (Fig. 1c) area. In the following days (from 13th to 18th July), the intrusion began shallower and, interacting with the fracture field opened on the first day of the eruption onset, fed the lava emission from the vent (LV) at 2100 m asl (just at the southern tip of the fracture field) from early 18th July. This occurrence was accompanied by a reduction of the tensile opening of the dike which passed from ~2.7 to ~1.7 m in the shallower portions.

In addition, ground deformation data detect a deflation volume located close to the summit area at a shallow depth (1.8 km bsl). After 17th July some vents (UV) opened along the western margin of the Valle del Bove and fed lava flows spreading into the Valle del Bove and over Piano del Lago (Lautze et al., 2004). Petrochemical studies carried out on the material erupted by these vents have inferred a petrologic composition close to the one detected for the products erupted during June–July 2001, evidencing that both magmas belong to the same shallow reservoir (Corsaro et al., 2013). In light of this, the shallow deflating sources detected by geodetic data for different time intervals (for *I3* and *I5*, respectively; during *I4* the ground deformation pattern is dominated by the intrusion onset) could represent adjacent portions of a shallow reservoir feeding both the activity that occurred at SEC (since January 2001) and the activity of the UV (during the July–August eruption). In particular, the drop in the pressure of this reservoir due to the magma drainage since June 2001 creates a pressure imbalance with a deeper magma source (presumably, the one active during *I1–I2*), motivating the ascent of fresh magma from the deep source into the reservoir, as evidenced by the slight compositional shift of the compositions toward a more primitive magma in the products erupted after June 2001 (Corsaro et al., 2013). Moreover, regional tectonics, related to N–S trending structures, also could have facilitated the ascent of magma toward the surface (*e.g.* Acocella and Neri, 2003).

Modelling of the ground deformation field measured from 18th July to 15th August (*I6*) infers a deflating source located beneath the upper southern flank of the volcano at a depth of ~7.2 km bsl. It must be noted that, although located at a similar depth, this (deflating) source is clearly distinct (based on the horizontal position and model uncertainties) from the (inflating) one modelled for intervals *I1–I2*. The depth inferred by modelling of geodetic data is in agreement with the depth range (5–12 km) estimated by analysing the petrochemical characteristics of the magma erupted by LV. In particular, Metrich et al. (2004) have pointed out that magma erupted by LV represents a magma that evolved under high pressure and possibly experienced a quick rise to the surface. Rapid magma uprising also was suggested as justification for the gravity increase observed close to the LV from 19th July to 2nd August 2001 (Carbone et al., 2003). Corsaro et al. (2007) found evidence that UV and LV magmas remain clearly distinct and ascended following different paths, ruling out the

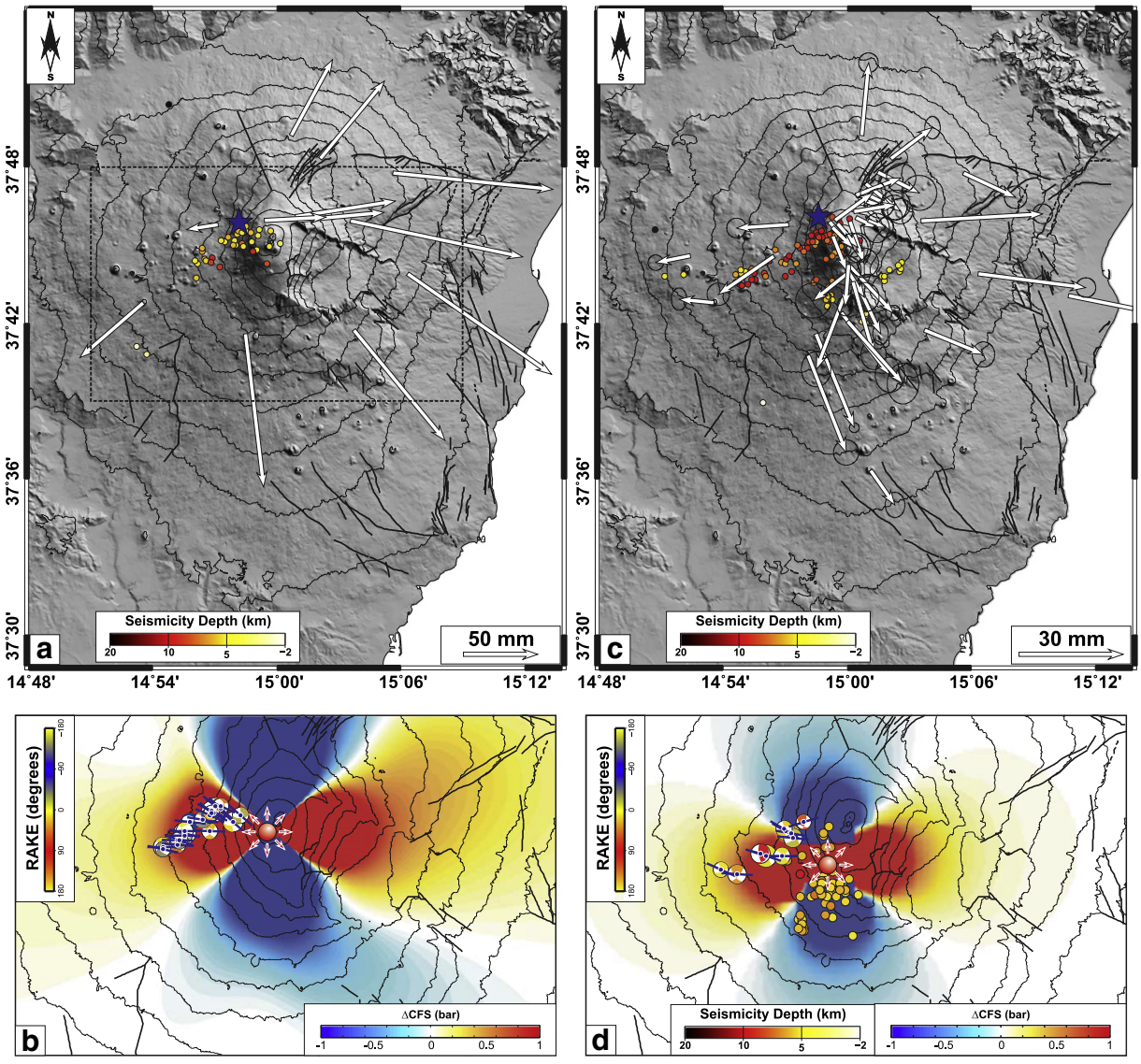

Fig. 7. a) Ground deformation field measured for September 1993–July 1997 period (Palano et al., 2008). Modelled source is reported as blue star. Earthquakes occurred during the 9th–14th January 1998 seismic swarm also are reported. Dashed box shows the area reported in panels b and d. b) Focal plane solutions (lower hemisphere projection) of well-constrained events occurring during the 9th–14th January 1998 seismic swarm (FPSs are coloured according to rake: red indicates pure thrust faulting, blue is pure normal faulting, and yellow is strike-slip faulting); blue lines represent the S_{Hmax} orientation computed for each FPS. The colour in background shows the CFS changes (at a depth of ~6.0 km bsl) as computed in Bonanno et al. (2011). c) Ground deformation field measured for *I1*. Modelled source (this study) is reported as a blue star. Earthquakes occurred during the 20th–24th April 2001 seismic swarm are also reported. d) Focal plane solutions (lower hemisphere projection) of well-constrained events occurring during the 20th–24th January 1998 seismic swarm (from Bonaccorso et al., 2004); blue lines represent the S_{Hmax} orientation computed for each FPS. Earthquakes that occurred during the May–June 2001 time interval also are reported. The colour in background shows the CFS changes (at a depth of 7.0 km bsl) due to a magmatic source characterized by an increase of volume of $2 \cdot 10^6$ m^3.

occurrence of mixing processes between them. However, despite petrologic and compositional differences between UV and LV magmas, the ratio of selected incompatible elements suggests that both derive from a common parental magma (Corsaro et al., 2013). In light of this, UV and LV magmas arise from a common source region (likely located at ~7 km bsl as evidenced by geodetic data) and ascend to the surface following different paths, experiencing degassing, cooling and crystallization at different P–T conditions.

5.3. The 2001 eruption: some constraints from the 1993–1998 time interval

The pre-eruptive period, particularly the 1-year period preceding the July–August 2001 eruption, seems to be of particular relevance. It appears to undergo some geophysical processes that resemble the ones occurring during the 1993–1998 time interval (Fig. 7):

(1) *Inflation of a magmatic source located beneath the western flank of the volcano*. After the end of the 1991–1993 eruption, Mt. Etna underwent a new marked inflation phase (see Palano et al., 2008 for an overview), evidencing the presence of a recharging reservoir located beneath its upper western flank at a depth of ~6.0 km bsl (Fig. 7a).

(2) *Seismic swarm beneath the western flank*. Starting from 1997, a sharp increase in seismicity affected the volcano with the occurrence of several swarms beneath its western flank. The strongest of them was recorded during 9th–14th January 1998 (maximum magnitude = 3.7; Bonanno et al., 2011).

Earthquake foci distribution depicted a marked alignment along a narrow volume *ca*. N50°E-oriented (Fig. 7a). Computed fault plane solutions showed predominant right-lateral strike-slip kinematic along the N50°E trend with a nodal plane striking almost parallel to this alignment; (Fig. 7a; Bonanno et al., 2011).

(3) *Shallow intrusion*. Ground deformation measurements covering the July 1997–July 1998 period detected a shallow intrusive episode: the inversion of geodetic data inferred two dikes, both west-dipping and located respectively beneath the summit area and the North-East rift (Palano et al., 2008). In addition, Bonanno et al. (2011) demonstrated that an inflationary source located beneath the upper southern flank at a depth of ~6.0 km bsl could trigger both the N50°E fault system to slip as a right-lateral strike-slip fault (Fig. 7b) and to intrude into a weak zone located at a depth lower than 3 km bsl.

5.4. Modelling changes in Coulomb stress

To confirm the hypothesis that seismic swarms beneath the western flank are a prevailing feature and likely linked to the variations in the crustal stressing-rate in the Mt. Etna magmatic feeding system, we perform a similar analysis as shown in Bonanno et al. (2011). In particular, we calculate the Coulomb Failure stress (CFS) changes induced by the deformation source on the western flank along the N50°E structural trend, assuming that as observed for the 9th–14th January 1998 period, this sector of the volcano is close to a critical state of failure. Following King et al. (1994) and Beeler et al. (2000) the Coulomb failure stress change is defined as:

$$\Delta CFS = \Delta\tau + \mu' \Delta\sigma_n \quad (1)$$

where $\Delta\tau$ is the shear stress change computed in the direction of slip on the fault, μ' is the effective friction [$\mu' = \mu(1 - B)$] and B is the Skempton parameter ($B = -\Delta P / \Delta\sigma_n$; $\Delta\sigma_n$ is the normal stress change, μ is the coefficient of friction and ΔP is the pore pressure change). To perform the CFS change computation we used the Coulomb 3.2 software (Toda et al., 2002). During the computation, we adopted the values of 30 GPa, 0.25 and 0.4 for shear modulus, Poisson's ratio and μ', respectively. As input we used a source spatially coincident with the deflating source inferred for the 18th July–15th August period but characterized by an increase of volume of $2–6 \cdot 10^6$ m^3. This volume change range is consistent with the maximum volume changes of a source at a 6–9 km depth, which could not be detected with InSAR considering the noise level in the interferogram after atmospheric correction, estimated about ~1.5 cm (see Fig. S2 reported in the Supplementary material). In spite of the low volume variation chosen (it represents only the ~20–46% of volume reduction estimated for the post-eruption deflation and generates small deformation on the surface in agreement with InSAR observations), we observed an increase in stress change (> 0.3–0.4 bar; Fig. 7d) on a large part of the N50°E fault system, supporting the hypothesis that the stress change increase produced by the pressurization of a source located beneath the upper southern flank of the volcano promoted the 20th–24th April 2001 seismic swarm as previously observed for the one occurred on 9th–14th January 1998 (Fig. 7b). A stress change increase along the N50°E structural trend due to a deep intrusion beneath the upper southern flank of Mt. Etna was suggested also by Mattia et al. (2007) as a result of the analysis of the seismicity recorded between November 2000 and April 2001. The agreement with previous analyses and the striking similarities with the 1998 seismic swarm strongly suggest the prevailing magmatic nature of the swarms beneath the western flank. As shown here, this N50°E fault zone might act as a stress gauge under the activation of this section of the magmatic feeding system of Mt. Etna.

6. Concluding remarks

Taking into account the results presented above and the volcanological, and seismological observations discussed here, we can draw the following conclusions:

(1) From July 2000 until 24th April 2001, geodetic data support the occurrence of magmatic recharge beneath the western flank of the volcano. It is likely that this recharge began in the fall of 2000, as evidenced by seismological and volcanological observations, but the lack of available continuous observations does not permit constraining this temporal relationship.

(2) The seismic swarm that occurred on 20th–24th April 2001 on the western flank of the volcano marked a clear change on the magmatic feeding system of Mt. Etna. Geodetic data detected only a slight contraction of the summit area, while no clear signal related to the activity of the deep inflating source inferred for the previous period can be easily recognized. We suggest that this source experienced a sharp reduction of the inflation rate in response to the seismic swarm beneath the western flank of the volcano. Moreover the beginning of a deep magmatic recharge phase beneath the upper southern flank cannot be ruled out, as previously observed for the 1997–1998 period (Bonanno et al., 2011). This fact also is corroborated by the occurrence of significant seismic activity beneath the upper southern flank of the volcano (average foci depth ~7 km bsl) during May–June 2001 and by the location of the deflating source inferred by geodetic data modelling that explains the post-intrusion deep deflation observed from 18th July to 15th August time interval. All these observations, coupled with petrochemical observations, suggest that magma emitted from LV probably arises from this source.

(3) On 12th July, the final phase of the intrusion began. The rapid depressurization of the magma reservoir due to the shallow dike intrusion induced the upward ascent of magma. Dike intrusion started at a shallow depth (~2.5 km bsl) and propagated toward the surface. From 13th to 18th July, geodetic data clearly show that the intrusion began shallower and, interacting with the fracture field at the volcano surface, fed some lava flows emitted from the vent (LV) that opened on early 18th July at 2100 m asl (just at the southern tip of the fracture field).

(4) Geodetic data also infer the presence of two deflating sources located at a shallow depth (~2 km bsl) beneath the summit area and that could represent adjacent portions of the same shallow reservoir feeding both the activity that has occurred at SEC since January 2001 and the activity of the UV during the 2001 eruption. The drop in pressure of this reservoir due to the magma drainage after June 2001 creates a pressure imbalance with the deeper magma source located beneath the western flank, motivating the ascent of fresh magma into the shallow reservoir.

This study presents an example of how a systematic revisit of past geodetic data using updated techniques can bring new insights into some well-known eruptions. A comprehensive revisit of the 2001 eruption of Mt. Etna data shows new evidence for the presence of a deep inflating source whose activity can produce a mechanical response of the western flank (April 2001 seismic swarm), producing a sharp change in the magmatic feeding system which culminated in the July–August eruption. This type of pattern, whose common features also were observed during the December 1991 and January 1998 in conjunction with seismic swarms (see Bonanno et al., 2011 for an overview), represents a prevailing pattern that could help to identify inflation phases of this portion of the magmatic feeding system of Mt. Etna. Such links between magmatic and local fault zones have been recognized at different volcano types in different regions and tectonic setting, suggesting that these interactions represent a

common pattern in active volcanoes and could be a helpful tool for the volcano monitoring.

Acknowledgements

We thank two anonymous reviewers and the Editor Jürgen W. Neuberg for their critical reviews and constructive comments that greatly improved the paper. We acknowledge Rosa Anna Corsaro and Amalia Bonanno for a fruitful discussion during the preparation of the manuscript, and Kristy F. Tiampo for a critical review of the preliminary draft. The CGPS group is kindly acknowledged for providing raw data. Pablo J. González thanks the support of a Banting Postdoctoral Fellowship by the Canadian Government. GMT software (http://gmt.soest.hawaii.edu) was used to create all figures.

Appendix A

As presented in the main text, the detected apparent phase change cannot be unequivocally interpreted as magmatic deformation signals and are more likely due to differential atmospheric delays. In the following, we detail the two independent correction models used to analyse possible atmospheric phase contributions for the selected differential interferogram (Fig. A1a).

Several methods using satellite spectroradiometry have been proposed based on MODIS (Li et al., 2005) and MERIS data (Puysségur et al., 2007). In 2001 only MODIS data from TERRA satellite were available for InSAR corrections. Precipitable water vapour products based on 1-km resolution MODIS near-infrared channels were obtained from the same day of the SAR image acquisitions. We reprojected them to a common geographical projection, and converted to slant wet delay maps consistent with the local incidence angle (Li et al., 2005). To avoid unreliable phase delay estimates over cloudy areas, a cloud mask at a 95% probability was applied. Subsequently, we linearly interpolate the phase delay over the masked areas. Finally, the delay maps were differentiated to obtain a correction model for the 6th June 2001–11th July 2001 interferogram (Fig. A1c).

A second correction approach was based on the computation of a differential delay map based on weather reanalysis models (Jolivet et al., 2011). For this study, we have used the ERA-Interim global reanalysis model. ERA-Interim is a global atmospheric model calculated by the ECMWF, European Centre for Medium-Range Weather Forecasts, which assimilates surface and satellite meteorological data. Data is

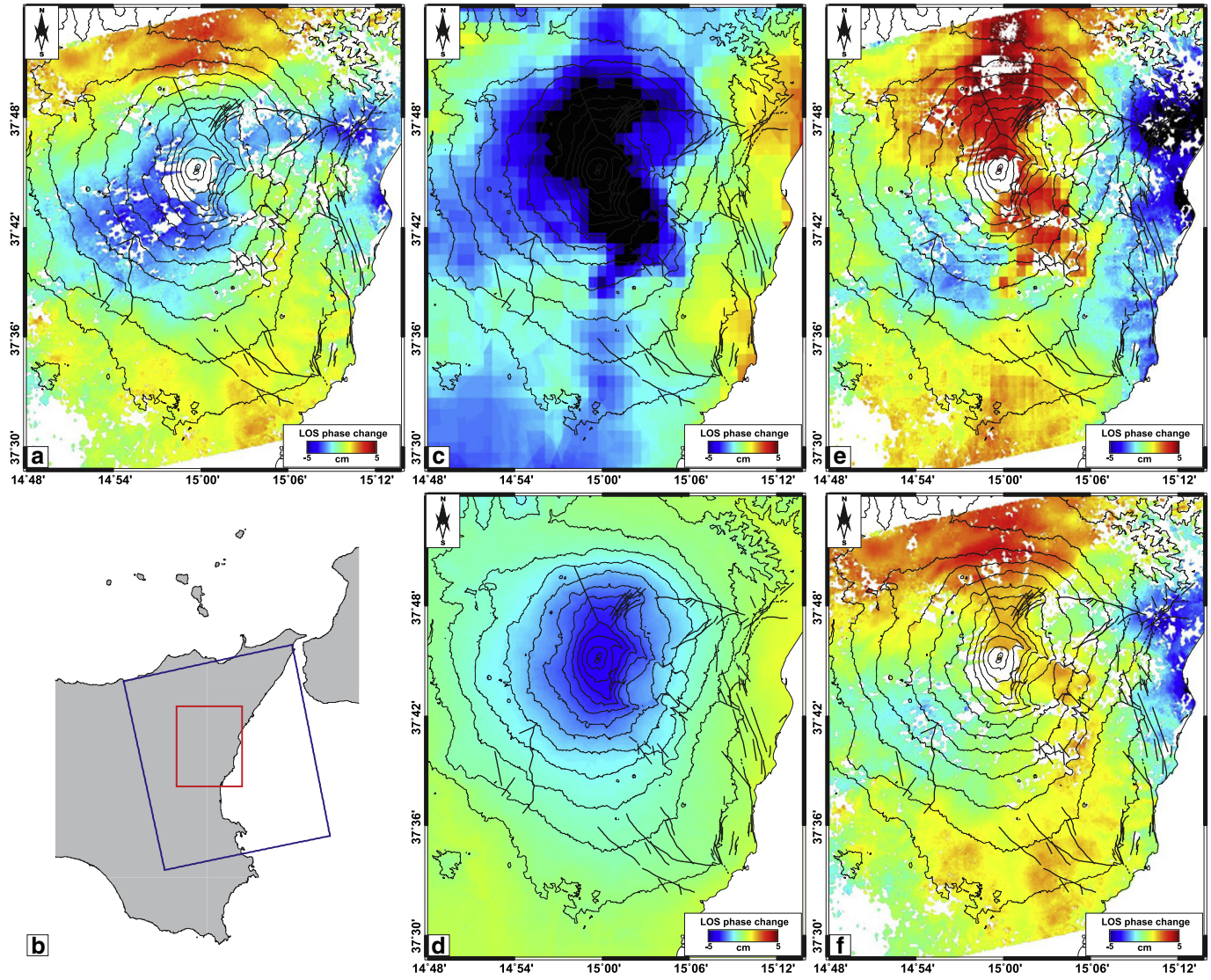

Fig. A1. a) InSAR data spanning the 6th June–11th July 2001 time interval. Areas which lack interferometric coherence are uncoloured. b) ERS-2 ascending satellite SAR images: blue and red boxes represent the footprint area illuminated by the SAR scenes (Track 129, Frame 747) and the area reported on panels a, c, d, e, and f of this figure, respectively. c) MODIS modelled delay maps; d) ERA-Interim modelled delay map; e) MODIS corrected differential phase map; f) ERA-Interim corrected differential phase map. We use the convention that negative motion is toward the satellite.

available from 1979 to the present, with a horizontal spatial resolution of 0.75-degrees on a gaussian reduced grid (~79 km), and a vertical resolution of 37 pressure levels, with the highest resolution at the planetary boundary layer. The model has a 6 hour temporal resolution, daily at 0:00, 6:00, 12:00 and 18:00 (www.ecmwf.int/research/era/do/get/era-interim). We follow the approach proposed by Jolivet et al. (2011) and implemented the package pyAPS (http://earthdef.caltech.edu/projects/pyaps/wiki/Main). We selected the 18:00 time resolution data, the closest to SAR acquisition times. Then, delay as a function of elevation is obtained on each grid node using temperature, water vapour and dry air partial pressure parameters (by cubic interpolation). Finally, continuous fine resolution delay maps were obtained by piecewise linear interpolation. The resulting ERA-Interim delay model for the 6th June 2001–11th July 2001 interferogram is reported in Fig. A1e.

Appendix B. Supplementary data

Supplementary data to this article can be found online at http://dx.doi.org/10.1016/j.jvolgeores.2014.02.001.

References

Acocella, V., Neri, M., 2003. What makes flank eruptions? The 2001 Etna eruption and its possible triggering mechanisms. Bull. Volcanol. 65 (7), 517–529. http://dx.doi.org/10.1007/s00445-003-0280-3.

Allard, P., Behncke, B., D'Amico, S., Neri, M., Gambino, S., 2006. Mount Etna 1993–2005: anatomy of an evolving eruptive cycle. Earth Sci. Rev. 78, 85–114. http://dx.doi.org/10.1016/j.earscirev.2006.04.002.

Aloisi, M., Cocina, O., Neri, G., Orecchio, B., Privitera, E., 2002. Seismic tomography of the crust underneath the Etna volcano, Sicily. Phys. Earth Planet. Inter. 134, 139–155. http://dx.doi.org/10.1016/S0031-9201(02)00153-X.

Aster, R., Borcher, B., Thurber, C.H., 2005. Parameter Estimation and Inverse Problems. Academic Press, International Geophysics Series (320 pp.).

Baker, S., Amelung, F., 2012. Top-down inflation and deflation at the summit of Kīlauea Volcano, Hawai'i observed with InSAR. J. Geophys. Res. 117, B12406. http://dx.doi.org/10.1029/2011JB009123.

Beauducel, F., Briole, P., Froger, J.-L., 2000. Volcano-wide fringes in ERS synthetic aperture radar interferograms of Etna (1992–1998): deformation or tropospheric effect? J. Geophys. Res. 105 (B7), 16391–16402. http://dx.doi.org/10.1029/2000JB900095.

Beeler, N.M., Simpson, R.W., Hickman, S.H., Lockner, D.A., 2000. Pore fluid pressure, apparent friction and Coulomb failure. J. Geophys. Res. 105, 25533–25542. http://dx.doi.org/10.1029/2000JB900119.

Behncke, B., Neri, M., 2003. The July–August 2001 eruption of Mt. Etna (Sicily). Bull. Volcanol. 65, 461–476. http://dx.doi.org/10.1007/s00445-003-0274-1.

Beutler, G., Moore, A.W., Mueller, I.I., 2008. The International Global Navigation Satellite Systems (GNSS) Service: developments and achievements. J. Geod. 83 (3–4), 297–307. http://dx.doi.org/10.1007/s00190-008-0268-z.

Boehm, J., Werl, B., Schuh, H., 2006. Troposphere mapping functions for GPS and very long baseline interferometry from European Centre for Medium-Range Weather Forecasts operational analysis data. J. Geophys. Res. 111, B02406. http://dx.doi.org/10.1029/2005JB003629.

Bonaccorso, A., Aloisi, M., Mattia, M., 2002. Dike emplacement forerunning the Etna July 2001 eruption modeled through continuous tilt and GPS data. Geophys. Res. Lett. 29 (13). http://dx.doi.org/10.1029/2001GL014397.

Bonaccorso, A., D'Amico, S., Mattia, M., Patanè, D., 2004. Intrusive mechanisms at Mt. Etna forerunning the July–August 2001 eruption from seismic and ground deformation data. Pure Appl. Geophys. 161, 1469–1487. http://dx.doi.org/10.1007/s00024-004-2515-4.

Bonaccorso, A., Currenti, G., Del Negro, C., Boschi, E., 2010. Dike deflection modelling for inferring magma pressure and withdrawal, with application to Etna 2001 case. Earth Planet. Sci. Lett. 293, 121–129. http://dx.doi.org/10.1016/j.epsl.2010.02.030.

Bonanno, A., Palano, M., Privitera, E., Gresta, S., Puglisi, G., 2011. Magma intrusion mechanisms and redistribution of seismogenic stress at Mt. Etna volcano (1997–1998). Terra Nova 23, 339–348. http://dx.doi.org/10.1111/j.1365-3121.2011.01019.x.

Bonforte, A., Bonaccorso, A., Guglielmino, F., Palano, M., Puglisi, G., 2008. Feeding system and magma storage beneath Mt. Etna as revealed by recent inflation/deflation cycles. J. Geophys. Res. 113, B05406. http://dx.doi.org/10.1029/2007JB005334.

Bruno, V., Mattia, M., Aloisi, M., Palano, M., Cannavò, F., Holt, W.E., 2012. Ground deformations and volcanic processes as imaged by CGPS data at Mt. Etna (Italy) between 2003 and 2008. J. Geophys. Res. 117, B07208. http://dx.doi.org/10.1029/2011JB009114.

Carbone, D., Budetta, G., Greco, F., 2003. Possible mechanisms of magma redistribution under Mt Etna during the 1994–1999 period detected through microgravity measurements. Geophys. J. Int. 153, 187–200. http://dx.doi.org/10.1046/j.1365-246X.2003.01901.x.

Carbone, D., D'Amico, S., Musumeci, C., Greco, F., 2009. Comparison between the 1994–2006 seismic and gravity data from Mt. Etna: new insight into the long-term behavior of a complex volcano. Earth Planet. Sci. Lett. 279, 282–292. http://dx.doi.org/10.1016/j.epsl.2009.01.007.

Cayol, V., Cornet, F.H., 1998. 3D modeling of the 1983–1984 eruption at Piton de la Fournaise volcano, Réunion Island, Indian Ocean. J. Geophys. Res. 103, 18025–18037.

Chiarabba, C., Amato, A., Boschi, E., Barberi, F., 2000. Recent seismicity and tomographic modeling of the Mount Etna plumbing system. J. Geophys. Res. 105 (B5), 10923–10938. http://dx.doi.org/10.1029/1999JB900427.

Corsaro, R., Miraglia, L., Pompilio, M., 2007. Petrologic evidence of a complex plumbing system feeding the July–August 2001 eruption of Mt. Etna, Sicily, Italy. Bull. Volcanol. 69 (4), 401–421. http://dx.doi.org/10.1007/s00445-006-0083-4.

Corsaro, R.A., Di Renzo, V., Distefano, S., Miraglia, L., Civetta, L., 2013. Relationship between petrologic processes in the plumbing system of Mt. Etna and the dynamics of the eastern flank from 1995 to 2005. J. Volcanol. Geotherm. Res. 251, 75–89. http://dx.doi.org/10.1016/j.jvolgeores.2012.02.010.

Delacourt, C., Briole, P., Achache, J., 1998. Tropospheric corrections of SAR interferogramms with strong topography. Application to Etna. Geophys. Res. Lett. 25, 2849–2852. http://dx.doi.org/10.1029/98GL02112.

Eff-Darwich, A., Pérez-Darias, J.C., Fernández, J., García-Lorenzo, B., González-Fernández, A., González, P.J., 2012. Using a mesoscale meteorological model to reduce the effect of tropospheric water vapour from DInSAR data: a case study for the Island of Tenerife, Canary Islands. Pure Appl. Geophys. 169 (8), 1425–1441. http://dx.doi.org/10.1007/s00024-011-0401-4.

Efron, B., 1982. The Jackknife, Bootstrap and Other Resampling Plans. Society for Industrial and Applied Mathematics, Philadelphia, PA.

Froger, J.-L., Merle, O., Briole, P., 2001. Active spreading and regional extension at Mount Etna imaged by SAR interferometry. Earth Planet. Sci. Lett. 187 (3–4), 245–258. http://dx.doi.org/10.1016/S0012-821X(01)00290-4.

Fukushima, Y., Cayol, V., Durand, P., Massonnet, D., 2010. Evolution of magma conduits during the 1998–2000 eruptions of Piton de la Fournaise volcano, Réunion Island. J. Geophys. Res. 115, B10204. http://dx.doi.org/10.1029/2009JB007023.

González, P.J., Samsonov, S., Pepe, S., Tiampo, K.F., Tizzani, P., Casu, F., Fernández, J., Camacho, A.G., Sansosti, E., 2013. Magma storage and migration associated with the 2011–2012 El Hierro eruption: implications for shallow magmatic systems at oceanic island volcanoes. J. Geophys. Res. Solid Earth 118, 4361–4377. http://dx.doi.org/10.1002/jgrb.50289.

Guglielmino, F., Bignami, C., Bonforte, A., Briole, P., Obrizzo, F., Puglisi, G., Stramondo, S., Wegmueller, U., 2011. Analysis of satellite and in situ ground deformation data integrated by the SISTEM approach: the April 3, 2010 earthquake along the Pernicana fault (Mt. Etna — Italy) case study. Earth Planet. Sci. Lett. 312 (3–4), 327–336. http://dx.doi.org/10.1016/j.epsl.2011.10.028.

Herring, T.A., King, R.W., McClusky, S.C., 2010. Introduction to GAMIT/GLOBK, Release 10.4. Massachusetts Institute of Technology, Cambridge MA 1–48.

Jolivet, R., Grandin, R., Lasserre, C., Doin, M.-P., Peltzer, G., 2011. Systematic InSAR tropospheric phase delay corrections from global meteorological reanalysis data. Geophys. Res. Lett. 38, L17311. http://dx.doi.org/10.1029/2011GL048757.

Kampes, B.M., Hanssen, R.F., Perski, Z., 2003. Radar interferometry with public domain tools. 3rd International Workshop on ERS SAR Interferometry, 'FRINGE03', Frascati, Italy, 1–5 Dec.

King, G.C.P., Stein, R.S., Lin, J., 1994. Static stress changes and the triggering of earthquakes. Bull. Seismol. Soc. Am. 84, 935–953.

Lanzafame, G., Neri, M., Acocella, V., Billi, A., Funicello, R., Giordano, G., 2003. Structural features of the July–August 2001 Mount Etna eruption: evidence for a complex magma supply system. J. Geol. Soc. Lond. 160, 531–544. http://dx.doi.org/10.1144/0016-764902-151.

Lautze, N.C., Harris, A.J.L., Bailey, J.E., Ripepe, M., Calvari, S., Dehn, J., Rowland, S.K., Evans-Jones, K., 2004. Pulsed lava effusion at Mount Etna during 2001. J. Volcanol. Geotherm. Res. 137, 231–246. http://dx.doi.org/10.1016/j.jvolgeores.2004.05.018.

Li, Z., Muller, J.-P., Cross, P., Fielding, E.J., 2005. Interferometric synthetic aperture radar (InSAR) atmospheric correction: GPS, Moderate Resolution Imaging Spectroradiometer (MODIS), and InSAR integration. J. Geophys. Res. 110 (B3), B03410. http://dx.doi.org/10.1029/2004JB003446.

Lisowski, M., Dzurisin, D., Denlinger, R.P., Iwatsubo, E.Y., 2008. Analysis of GPS-measured deformation associated with the 2004–2006 dome-building eruption of Mount St. Helens, Washington. In: Sherrod, R.D., Scott, W.E., Stauffer, P.H. (Eds.), A Volcano Rekindled: the Renewed Eruption of Mount St. Helens, 2004–2006. USGS. Prof. Pap., 1750, pp. 301–333.

Lundgren, P., Rosen, P.A., 2003. Source model for the 2001 flank eruption of Mt. Etna volcano. Geophys. Res. Lett. 30 (7), 1388. http://dx.doi.org/10.1029/2002GL016774.

Lundgren, P., Casu, F., Manzo, M., Pepe, A., Berardino, P., Sansosti, E., Lanari, R., 2004. Gravity and magma induced spreading of Mount Etna volcano revealed by satellite radar interferometry. Geophys. Res. Lett. 31, L04602. http://dx.doi.org/10.1029/2003GL018736.

Martinez-Arevalo, C., Patanè, D., Rietbrock, A., Ibanez, J.M., 2005. The intrusive process leading to the Mt. Etna 2001 flank eruption: constraints from 3-D attenuation tomography. Geophys. Res. Lett. 32, L21309. http://dx.doi.org/10.1029/2005GL023736.

Mattia, M., Patanè, D., Aloisi, M., Amore, M., 2007. Faulting on the western flank of Mt Etna and magma intrusions in the shallow crust. Terra Nova 19, 89–94. http://dx.doi.org/10.1111/j.1365-3121.2006.00724.x.

McTigue, F.D., 1987. Elastic stress and deformation near a finite spherical magma body: resolution of the point source paradox. J. Geophys. Res. 92 (B12), 12931–12940. http://dx.doi.org/10.1029/JB092iB12p12931.

Metrich, N., Allard, P., Spilliaert, N., Andronico, D., Burton, M., 2004. 2001 flank eruption of the alkali- and volatile-rich primitive basalt responsible for Mount Etna's evolution in the last three decades. Earth Planet. Sci. Lett. 228, 1–17. http://dx.doi.org/10.1016/j.epsl.2004.09.036.

Mogi, K., 1958. Relation between the eruptions of various volcanoes and the deformations of the ground surfaces around them. Bull. Earthq. Res. Inst. Univ. Tokyo 36, 99–134.

Montgomery-Brown, E.K., Sinnett, D.K., Larson, K.M., Poland, M.P., Segall, P., Miklius, A., 2011. Spatiotemporal evolution of dike opening and décollement slip at Kīlauea Volcano, Hawai'i. J. Geophys. Res. 116, B03401. http://dx.doi.org/10.1029/2010JB007762.

Okada, Y., 1985. Surface deformation due to shear and tensile fault in half-space. Bull. Seismol. Soc. Am. 75, 1135–1154.

Palano, M., Puglisi, G., Gresta, S., 2008. Ground deformation patterns at Mt. Etna from 1993 to 2000 from joint use of InSAR and GPS techniques. J. Volcanol. Geotherm. Res. 169 (3–4), 99–120. http://dx.doi.org/10.1016/j.jvolgeores.2007.08.014.

Palano, M., Rossi, M., Cannavò, C., Bruno, V., Aloisi, M., Pellegrino, D., Pulvirenti, M., Siligato, G., Mattia, M., 2010. Etn@ref, a geodetic reference frame for Mt. Etna GPS networks. Ann. Geophys. 53 (4), 48–79. http://dx.doi.org/10.4401/af-4879.

Palano, M., Guarrera, E., Mattia, M., 2012. GPS ground deformation patterns at Mount St. Helens (Washington, USA) from 2004 to 2010. Terra Nova 24, 148–155. http://dx.doi.org/10.1111/j.1365-3121.2011.01049.x.

Pascal, K., Neuberg, J., Rivalta, E., 2013. On precisely modelling surface deformation due to interacting magma chambers and dykes. Geophys. J. Int.. http://dx.doi.org/10.1093/gji/ggt343.

Patanè, D., Privitera, E., Gresta, S., Akinci, A., Alparone, S., Barberi, G., Chiaraluce, L., Cocina, O., D'Amico, S., De Gori, P., Di Grazia, G., Falsaperla, S., Ferrari, F., Gambino, S., Giampiccolo, E., Langer, H., Maiolino, V., Moretti, M., Mostaccio, A., Musumeci, C., Piccinini, D., Reitano, D., Scarfì, L., Spampinato, S., Ursino, A., Zuccarello, L., 2003. Seismological constraints for the dike emplacement of July–August 2001 lateral eruption at Mt. Etna volcano, Italy. Ann. Geophys. 46 (4), 599–608.

Puglisi, G., Bonforte, A., Ferretti, A., Guglielmino, F., Palano, M., Prati, C., 2008. Dynamics of Mount Etna before, during, and after the July–August 2001 eruption inferred from GPS and differential synthetic aperture radar interferometry data. J. Geophys. Res. 113, B06405. http://dx.doi.org/10.1029/2006JB004811.

Puysségur, B., Michel, R., Avouac, J.-P., 2007. Tropospheric phase delay in interferometric synthetic aperture radar estimated from meteorological model and multispectral imagery. J. Geophys. Res. 112, B05419. http://dx.doi.org/10.1029/2006JB004352.

Rosen, P.A., Henley, S., Peltzer, G., Simons, M., 2004. Updated repeat orbit interferometry package released. EOS Trans. Am. Geophys. Union 85 (5), 47. http://dx.doi.org/10.1029/2004EO005004.

Saastamoinen, J., 1972. Contribution to the theory of atmospheric refraction. Bull. Géodésique 105 (1), 279–298. http://dx.doi.org/10.1007/BF02521844.

Saraò, A., Cocina, O., Privitera, E., Panza, G.F., 2010. The dynamics of the 2001 Etna eruption as seen by full moment tensor analysis. Geophys. J. Int. 181, 951–965. http://dx.doi.org/10.1111/j.1365-246X.2010.04547.x.

Solaro, G., Acocella, V., Pepe, S., Ruch, J., Neri, M., Sansosti, E., 2010. Anatomy of an unstable volcano from InSAR: multiple processes affecting flank instability at Mt. Etna, 1994–2008. J. Geophys. Res. 115, B10405. http://dx.doi.org/10.1029/2009JB000820.

Tiampo, K.F., Rundle, J.B., Fernandez, J., Langbein, J.O., 2000. Spherical and ellipsoidal volcanic sources at Long Valley caldera, California, using a genetic algorithm inversion technique. J. Volcanol. Geotherm. Res. 102, 189–206. http://dx.doi.org/10.1016/S0377-0273(00)00185-2.

Toda, S., Stein, R.S., Sagiya, T., 2002. Evidence from the AD 2000 Izu islands earthquake swarm that stressing rate governs seismicity. Nature 49, 58–61. http://dx.doi.org/10.1038/nature00997.

Trasatti, E., Giunchi, C., Bonafede, M., 2003. Effects of topography and rheological layering on ground deformation in volcanic regions. J. Volcanol. Geotherm. Res. 122, 89–110. http://dx.doi.org/10.1016/S0377-0273(02)00473-0.

Walter, T.R., Acocella, V., Neri, M., Amelung, F., 2005. Feedback processes between magmatic events and flank movement at Mount Etna (Italy) during the 2002–2003 eruption. J. Geophys. Res. 110, B10205. http://dx.doi.org/10.1029/2005JB003688.

Williams, C.A., Wadge, G., 2000. An accurate and efficient method for including the effects of topography in three-dimensional elastic models of ground deformation with applications to radar interferometry. J. Geophys. Res. 105 (B4), 8103–8120. http://dx.doi.org/10.1029/1999JB900307.

Yang, X.-M., Davis, P.M., Dieterich, J.H., 1988. Deformation from inflation of a dipping finite prolate spheroid in an elastic half-space as a model for volcanic stressing. J. Geophys. Res. 93, 4249–4257.